Carbon 107 (2016) 629–637

Contents lists available at ScienceDirect

Carbon

journal homepage: www.elsevier.com/locate/carbon

Nitrogen-enriched meso-macroporous carbon fiber network as a binder-free flexible electrode for supercapacitors

Lei Fan [a, b], Li Yang [a], Xiangying Ni [a], Jie Han [a, *], Rong Guo [a, **], Chuanfang (John) Zhang [c, ***]

[a] School of Chemistry and Chemical Engineering, Yangzhou University, Yangzhou, 225002, China
[b] Key Laboratory of Advanced Energy Materials Chemistry (Ministry of Education), Nankai University, Tianjin, 300071, China
[c] Centre for Research on Adaptive Nanostructures and Nanodevices (CRANN), Advanced Materials and BioEngineering Research (AMBER), School of Chemistry, Trinity College Dublin, Dublin 2, Ireland

ARTICLE INFO

Article history:
Received 22 April 2016
Received in revised form
16 June 2016
Accepted 18 June 2016
Available online 18 June 2016

ABSTRACT

In order to maximize supercapacitor performances, it is essential to engineer the electrode architecture with shortened ion-diffusion paths and high content of pseudocapacitive sites. By incorporating redox-active species into low-dimensional carbon materials, both the specific capacitances and rate capabilities can be improved. In this study, a self-sustaining, flexible mat consisting of nitrogen-enriched carbon fiber (NCF) network was successfully produced through the co-electrospinning of a polyacrylonitrile (PAN)/polyvinylpyrrolidone (PVP)/SiO_2 blended solution, followed by pyrolysis and SiO_2 removal processes. Despite its low surface area (<60 m^2/g), the NCF exhibits high nitrogen content (17.3 wt%) and interconnected meso-macroporous nanostructure, resulting in high pseudocapacitance (242 F/g at 0.2 A/g), fast rate capability, and excellent cycling performance (99% of initial capacitance after 5000 cycles). The electrical double-layer capacitance and pseudocapacitance can be easily decoupled. The binder-free NCF based symmetric supercapacitor demonstrates a purely capacitive responses and high rate handling. We attribute the excellent electrochemical performances to the good conductivity and shortened ion diffusion paths of carbon fiber backbone, and pseudocapacitive edge-concentrated nitrogen species.

© 2016 Published by Elsevier Ltd.

1. Introduction

Electrochemical capacitors, also called supercapacitors, are important energy storage devices which could provide much higher power density than Li-ion batteries and higher energy density than conventional capacitors [1]. Due to their high electrical conductivity, excellent chemical stability and high surface area, carbon materials have been extensively studied as the supercapacitor electrodes [2–8]. However, their derived double-layer capacitances were far from satisfied and greatly limited the energy density of the supercapacitor device [9]. It is generally accepted that either through shortening the ion diffusion paths or incorporating highly reversible redox sites, could greatly promote the rate-response as well as the pseudocapacitance [10–17].

As a novel kind of one-dimensional (1D) carbon structure, carbon fiber (CF) possesses large aspect ratio, high electrical conductivity and excellent mechanical stability [18–20]. However, due to its low surface area, CF usually displayed undesirable double-layer capacitance [19]. Doping nitrogen species to CF could incorporate pseudocapacitance without compromising the conductivity of the CF backbone [21–23]. Among various doping methods, pyrolysis of electrospun polymer fibers represents a facile route to fabricate a self-sustain, flexible nitrogen-doped carbon fiber (NCF) network in-situ with shortened ion diffusion path and good electrical conductivity [21,24,25]. Based on the electrostatic force and viscos counter-force, the fiber formation could be easily achieved by applying voltage [26,27]. The diameter, conductivity and other physical properties of the as-obtained NCF could be fairly changed through controlling the parameters such as polymer precursors or

* Corresponding author.
** Corresponding author.
*** Corresponding author.
E-mail addresses: hanjie@yzu.edu.cn (J. Han), guorong@yzu.edu.cn (R. Guo), zhangjc@tcd.ie (C. Zhang).

http://dx.doi.org/10.1016/j.carbon.2016.06.067
0008-6223/© 2016 Published by Elsevier Ltd.

compositions, conditions of electrospinning (voltage, inject speed and distance to the Al collector) as well as pyrolysis (temperature, time, etc) [26]. Polyacrylonitrile (PAN) is known for it good spinnability in solution and high carbon yield [26,28]. Unlike other thermoplastic polymers, the thermally-stable PAN fibers can well maintain the fibrous structure after pyrolysis, thus has been frequently selected as the source for both carbon and nitrogen in processing NCF [18,21,23]. It's worth mentioning that the doped nitrogen content highly depends on the carbonization/activation conditions [18,21,29]. For example, Beguin et al. found the nitrogen content reached a maximum 13 wt% at the optimized carbonization temperature of 700 °C [21].

Beside the nitrogen-doping, the porous structure of the CF is also of critical importance to the fast rate-response as well as high capacitance [18,21,30,31]. Recently, Ahn et al. prepared SnO_2-doped CF through a co-electrospinning process, followed by hydrogenation and removal of the Sn nanoparticles in acid solution. The as-obtained activated CF possessed surface area of 1082 m^2/g and showcased high pseudocapacitance (289 F/g at 10 mV/s) [31]. Although engineering high surface area CF could promote the gravimetric double-layer capacitance, it would negatively affect the bulk density and the volumetric capacitance as a result. On the other hand, by utilizing low surface area NCF as electrodes, one could synergistically explore the advantages from the one-dimensional (1D) backbone with shortened ion diffusion paths, higher bulk density of the NCF and the nitrogen-induced pseudocapacitance. However, reports on the low surface area NCF as supercapacitor electrode are quite rare, to the best of our knowledge [32,33].

Herein, we have synthesized meso-macroporous NCF (up to 17.3 wt% nitrogen) with a low surface area (<60 m^2/g) through co-electrospinning of polymer/SiO_2 blended solution, followed by pyrolysis and SiO_2 removal processes. Effects of SiO_2 content as well as carbonization temperature on the NCF's physical and electrochemical properties have been systematically investigated. Electrochemical performances of the symmetric device based on the NCF binder-free electrodes have also been studied.

2. Experimental

2.1. Materials

Polyacrylonitrile (PAN, M_w ~150,000 g/mol), polyvinylpyrrolidone (PVP, M_w ~1,300,000 g/mol), N,N'-dimethylformide (DMF), Tetraethyl orthosilicate (TEOS), ammonium ($NH_3 \cdot H_2O$) were all purchased from Sigma–Aldrich and used as received. SiO_2 nanospheres were synthesized according to the literature [34]. Typically, 74 mL ethanol, 10 mL water and 3 mL $NH_3 \cdot H_2O$ were mixed and stirred for 1 h. Then, 6 mL TEOS was added into the solution and stirred for another 3 h at 50 °C. After centrifuging at 7000 rpm for 10 min, the sediment was collected, washed thoroughly with distilled water and ethanol alternatively for 3 times, and then dried at 70 °C for 12 h.

2.2. Electrospinning of SiO_2-embedded polymer microfibers

The precursor solution was prepared by mixing 66 wt% of the as-prepared SiO_2 nanospheres, 17 wt% PVP and 17 wt% PAN in DMF, followed by sonication for 4 h. The solution was fed into a syringe with outlet diameter of 0.6 mm. The ejected microfiber was received on the rotating collector covered by Al foil. During electrospinning, the applied voltage, distance, and flow rate were controlled at 15 kV, 15 cm, and 0.2 mm/min, respectively. The SiO_2 nanosphere content in the polymer solution (including PVP and PAN) was also varied at 0% SiO_2, 33% SiO_2, 50% SiO_2, or 75% SiO_2. In all polymer solutions, the weight percent of PVP and PAN was kept the same.

2.3. Synthesis of carbon fibers

The electrospun polymer fiber/SiO_2 mat was stabilized in an N_2 atmosphere at 250 °C for 1 h with a ramping rate of 1 °C/min, and then heated up to 800 °C for 2 h at a rate of 5 °C/min. The carbonized mats were then soaked in 1 M NaOH for 1 h, rinsed in deionized water until pH = 7, and finally dried for 12 h at 80 °C. The obtained sample was denoted as NCF-66% SiO_2. Similarly, other carbon fiber samples were denoted as NCF-0% SiO_2, NCF-33% SiO_2, NCF-50% SiO_2, or NCF-75% SiO_2, respectively. The polymer fiber mats (66% SiO_2) were also carbonized at 600 °C, 700 °C, 900 °C for 2 h, respectively. Unless specifically noted, the typical NCF indicates NCF-66% SiO_2 carbonized at 800 °C.

2.4. Characterization

The morphology, structure, composition, and surface chemistry were characterized by field-emission scanning electron microscopy (SEM, Hitachi S-4800, Japan), transmission electron microscopy (TEM, Tecnai-12 Philip Apparatus Co., USA), X-ray powder diffraction (XRD), energy dispersive X-ray spectroscopy (EDX, Brucker Quantax), Raman spectroscopy (Renishaw inVia Spectrometer), X-ray photoelectron spectroscopy (XPS, Thermo ESCALAB 250 spectrometer) and Fourier transform infrared spectroscopy (FTIR, Bruker Spectroscopy Instrument). Following gas sorption analysis (Thermo Sorptomatic 1990), the specific surface area was calculated using the Brunauer–Emmett–Teller (BET) method and the pore size distribution was derived from the Barrett-Joyner-Halenda (BJH) method. Elemental analysis was acquired using a Vario EL cube elemental analyzer.

2.5. Electrochemical measurements

The electrochemical performances of NCF were evaluated in a three-electrode setup in Swagelok® cells with Celgard 3501 as the separator. The freestanding NCF mat was punched into electrodes with 1 mg in weight and 8 mm in diameter. Counter electrodes were prepared from YP-50F activated carbon (Kuraray, Japan, SSA = 1470 m^2/g and pore diameter = 0.85 nm) by mixing the activated carbon with polytetrafluoroethylene (PTFE, 60 wt%) in a mass ratio of 95:5 in ethanol solution. Each YP-50F electrode was 15 mg. Ag/AgCl was used as the reference electrode, while 1 M H_2SO_4 was used as the electrolyte. Cyclic voltammograms (CV) at various sweep rates (5–100 mV/s) and galvanostatic charge/discharge (GCD) at different current densities (0.2–5 A/g) were performed on VMP3 (Biologic, France). Electrochemical impedance spectroscopy (EIS) was conducted at open-circuit potential (OCV). All the cells were cycled for 20 times at 20 mV/s for stabilization. In the three-electrode configuration, the specific capacitance was calculated from the discharge curve according to Equation (1):

$$C_{spe} = \frac{i}{m \times \frac{\Delta V}{\Delta t}} = \frac{j}{\frac{\Delta V}{\Delta t}} \quad (1)$$

where C_{spe} (F/g), m (g), j (A/g), Δt (s), ΔV (V) are, respectively: specific capacitance, mass of the working electrode, current density, discharge time, and potential window after the IR drop. In the two-electrode device, the specific capacitance was calculated from the CV integration according to Equation (2):

$$C_{spe} = \frac{2\int idV}{vm\Delta V} \quad (2)$$

where m is mass of one electrode, v is the scan rate, and C_{spe} is the gravimetric capacitance per electrode. Specific capacitance was also derived from the discharge curve of the symmetric device according to Equation (3):

$$C_{spe} = \frac{4i}{m' \times \frac{\Delta V}{\Delta t}} \quad (3)$$

where m' is the total electrode mass in the device.

3. Results and discussion

The preparation of a flexible NCF mat is presented in Fig. 1. First, the pale yellow blended solution (PAN/PVP/SiO_2) was electrospun into a randomly oriented polymer fiber mat decorated homogeneously with SiO_2 nanospheres (Fig. 1a), forming a wrinkled surface, as seen in the SEM and TEM images (Fig. 1b–c). Further carbonizing the polymer fiber mat produces a nitrogen-enriched carbon fiber mat (Fig. 1d), with visible voids appearing among the spherical SiO_2 nanospheres (Fig. 1e–f). Upon NaOH etching, the SiO_2 nanospheres were effectively removed, resulting in NCF with conjugated surfaces and an interconnected macroporous structure (Fig. 1g), as seen in the SEM and TEM images in Fig. 1h–i. The TEM image of the NCF in higher magnification could be seen in Fig. S1. After pyrolysis, the electrospun polymer changes to disordered carbon without obvious lattice fringes, demonstrating the amorphous nature in the carbonized sample. We note that the uniform distribution of SiO_2 nanospheres is of critical importance in preventing the polymer fibers from fusion and shrinking during the pyrolysis treatment. In fact, when electrospinning the PVP/PAN-only polymer solution without blending with SiO_2 nanospheres, the resulted fiber mat exhibits a smooth, non-porous "solid" surface with numerous merged and entangled bundles (Fig. S2), whose morphology resembles that of merged carbon fibers synthesized by Lin *et al* [18].

Fig. 2a shows the surface chemistry of three fiber mats (polymer, carbonized, and etched mats). In the polymer mat, peaks centered at 1440 cm^{-1} and 1595–1670 cm^{-1} correspond to the characteristic stretching vibrations from *C*–H and C=O, respectively [35]. Peaks at 804–1111 cm^{-1} are due to the stretching vibration of Si–O–Si [35]. While the intensity of C=O is greatly reduced after pyrolysis, it appears again after soaking the carbonized mat in NaOH solution, suggesting that the carboxylic groups in the etched mat primarily originate from the hard template etching treatment [8]. In addition, the absence of the Si–O–Si peak suggests that the SiO_2 nanospheres were effectively removed in the etched mat (NCF-66% SiO_2). This was further verified by TGA, in which ash content was 1.4% (Fig. 2b), and EDX results, in which no Si signals were presented (Fig. S3a). We further conducted XPS to obtain information about oxygen and nitrogen functionalities. Binding energy values were calibrated by using the graphitic C 1 s peak at 285 eV as the reference. In the XPS survey spectrum of NCF-66% SiO_2, only C 1 s, N 1 s, and O 1 s were observed (Fig. 2c). The core level of the N 1 s XPS spectrum displayed three peaks, located at 398.3 eV, 400.1 eV and 401.2 eV, corresponding to pyridinic-N (N-6), pyrrolic-N (N-5) and quaternary N (N-Q), respectively (Fig. 2d), with N-6 being the most prominent form in the NCF [36]. Fig. 2e shows the Raman spectrum of NCF-66% SiO_2. Two characteristic peaks at 1354 cm^{-1} and 1580 cm^{-1} correspond to the D peak and G peak, respectively. The prominent D peak suggests substantial defects in the NCF. Fig. S3b shows the XRD patterns of NCF-66% SiO_2 and NCF-0% SiO_2, with broad diffraction peaks that are indicative of amorphous NCF. Fig. 2f shows the nitrogen adsorption-desorption isotherms of NCF-0%

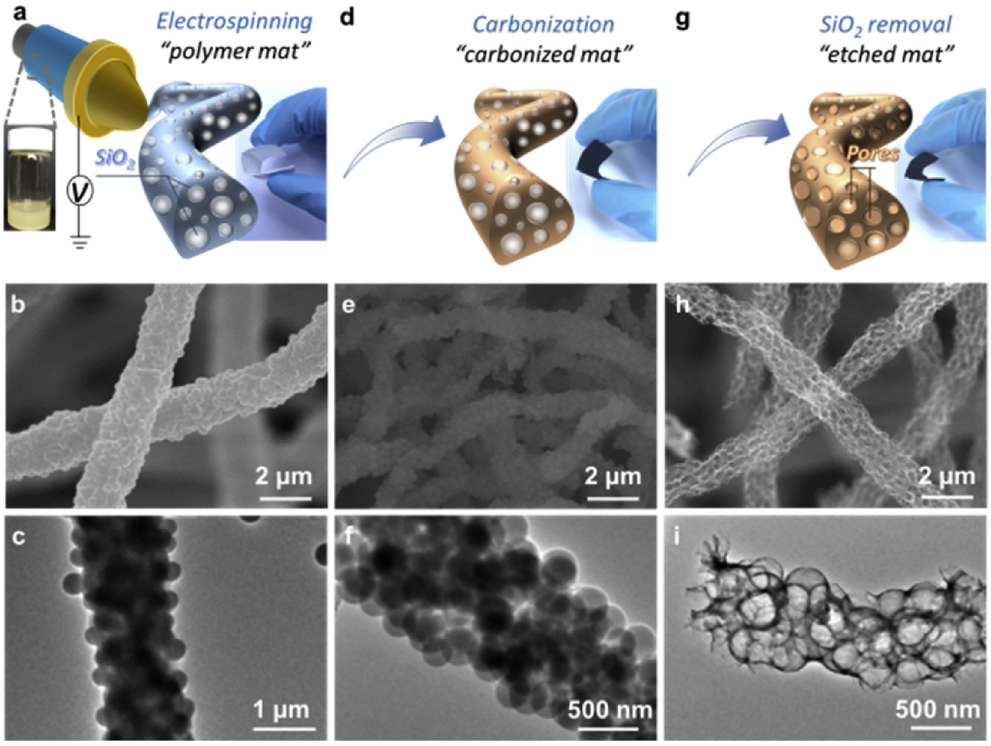

Fig. 1. Fabrication schematic of NCF mat and related (b,e,h) SEM and (c,f,i) TEM patterns. (a,b,c) PAN/PVP/SiO_2 polymer fibers; (d,e,f) carbon/SiO_2 carbonized fibers; (g,h,i) NCF fibers. (A colour version of this figure can be viewed online.)

and −66% SiO_2. Both NCF samples exhibit typical type-IV isotherms with a H_2 hysteresis loop at $P/P_0 = 0.9$, corresponding to a substantial amount of large mesopores. Combining the TEM results (Fig. 1i), which show substantial macropores in the NCF, it is reasonable to conclude that nitrogen-enriched carbon fibers with meso-macroporous nanostructure have been obtained through a co-electrospinning/hard template strategy. The absence of micropores lead to low specific surface area (SSA) in these NCF. Table S1 lists the porosity parameters of several NCF samples. Specifically, the BET specific surface area and pore volume of NCF-66% SiO_2 were 57 m^2/g and 0.26 cm^3/g, which represent about a six and two fold increase, respectively, compared to NCF-0% SiO_2.

Fig. 3 shows the electrochemical performances of NCF-0% SiO_2 and NCF-66% SiO_2. NCF-0% SiO_2 displays a quasi-rectangular CV curve (Fig. 3a) and a linear galvanostatic charge-discharge (GCD) profile (Fig. 3b), indicating highly capacitive behavior. Compared to NCF-0% SiO_2, NCF-66% SiO_2 exhibits a much larger encircled CV area and longer discharge time, suggesting substantial promoted specific capacitance (C_{spe}). To quantitatively prove this, a series of GCD tests at different specific currents were conducted for both samples (Fig. S4). The gravimetric capacitance was derived from the discharge profile based on Equation (1). As seen in Fig. 3c, at 0.2 A/g, C_{spe} of NCF-66% SiO_2 reaches 242 F/g, which is 6.5 times higher than that of NCF-0% SiO_2. When the specific current is increased by 10-fold, NCF-66% SiO_2 still exhibits 176 F/g (capacitance retention is 79%), which is almost 30 times higher than that of NCF-0% SiO_2. As the nitrogen content in these two samples is similar, the much enhanced capacitance and rate capability can be credited to the advantageous meso-macroporous nanostructure, which effectively facilitates the ion diffusion into the active sites for fast redox reactions [37]. According to Barbieri et al., the specific capacitance of the carbon-based nanomaterials increases linearly when scaling up the SSA to 1200 m^2/g [9]. Compared to commercial YP-50F or activated graphene, which exhibit S_{BET} ~3000 m^2/g, the low SSA (<60 m^2/g) of NCF-66% SiO_2 corresponds to a negligible capacitance (~8 F/g) according to Barbieri *et al* [9]. On the other hand, the redox reactions from the functionalities (nitrogen and oxygen species) greatly contributed to the capacitance of NCF-66% SiO_2. This finding distinguishes from other reported nanostructures, whose double-layer capacitance mixed with pseudocapacitance and one has to rely on ion kinetics analysis to determine each component's contribution [37,38]. Despite its low surface area, our meso-macroporous NCF still exhibits specific capacitance quite comparable to other nitrogen- (and/or oxygen-) enriched porous carbon [21,39–43]. Moreover, increasing the scan rate up to 100 mV/s results in the maintenance of a rectangular shape CV of NSF-66% SiO_2, without deviation, which is indicative of pseudocapacitive and fast rate responses (Fig. 3d). The electrochemical impedance

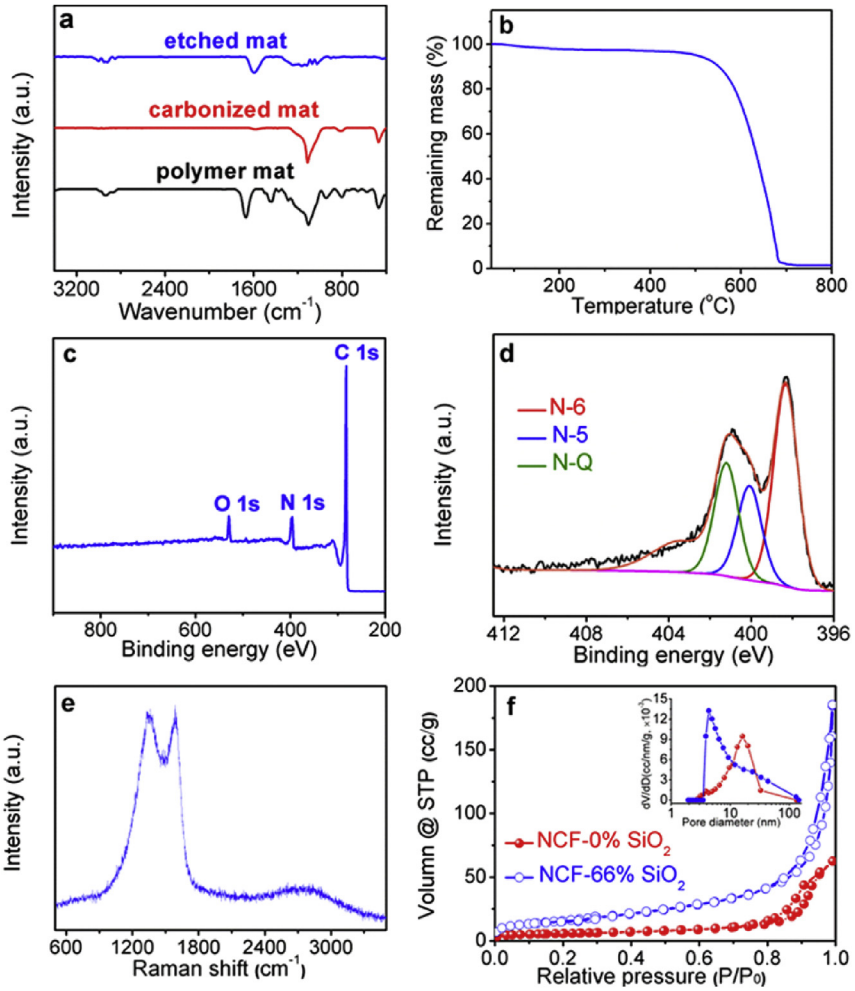

Fig. 2. (a) FTIR pattern for products at different stages. (b) TGA curve of NCF-66% SiO_2. (c) XPS survey spectra of NCF-66% SiO_2. (d) High-resolution XPS spectra of the deconvoluted N 1 s peak. (e) Raman pattern for NCF-66% SiO_2. (f) N_2 sorption isotherms of NCF-0% SiO_2 and NCF-66% SiO_2 with the inset displaying the corresponding pore size distribution curves. (A colour version of this figure can be viewed online.)

spectroscopy results (EIS) in Fig. 3e indicate a smaller semi-circle (about 0.6 Ω) and a more vertical line at low frequencies in NCF-66% SiO_2. This suggests faster ion transport and a highly conductive network that facilitates charge and ion percolation in the meso-macroporous NCF. As a result, the NCF-66% SiO_2 demonstrates excellent cycling lifetime. After soaking in the electrolyte for 24 h, the electrode exhibits a quite stable cycle life and retains 99% of the initial capacitance after 5000 cycles, as depicted in Fig. 3f.

We further investigate the effect of SiO_2 nanosphere content on the fibers' morphology and porosity, as well as the electrochemical performances. To achieve this, we adjusted the weight percent of SiO_2 nanospheres in the blended polymer solution to 33%, 50%, and 75%, respectively, while keeping the carbonization temperature constant (800 °C). The isotherms of several NCFs (Fig. S5) and their derived porosity parameters (Table S1) indicate that all NCFs are meso-macroporous with relatively low SSAs and pore volumes. The SEM and the TEM images in Fig. 4 and Fig. S6 show that the SiO_2 nanospheres are uniformly attached to the surface of the carbonized fibres. Upon the removal of the SiO_2 template, macropores were clearly observed (Fig. 4 e–h). In all cases, these ultra-long fibers were well separated from each other. The fiber diameter distribution and the mean values in several NCF samples can be seen in Fig. S7 and Table S1, respectively. For example, the average fiber diameter in NCF-33% SiO_2 is 970 nm, and increases to 3.3 μm in NCF-75% SiO_2. As a result, the electrochemical performances of these fibers also changed. Fig. 5a shows the CVs of NCFs at 10 mV/s, demonstrating pseudocapacitive behavior in all samples. An apparent increase in specific capacitance is observed in Fig. 5b as increasing the SiO_2 nanospheres content from 33% to 66%. The same trend in the EIS Nyquist plot (Fig. S8) implies that higher charge transfer resistance (R_{ct}) might be the reason for low capacitance in NCF-33% SiO_2. When the precursor contains excessive SiO_2 nanospheres, as in NCF-75% SiO_2, the increased fiber diameter (3.3 μm) leads to higher resistance (Fig. S8) and decreased specific capacitance (Fig. 5b).

In addition to the SiO_2 nanosphere content, we also explored the effect of carbonization temperature (T_c) on the electrochemical and physical properties of the NCFs. The XRD patterns are indeed featureless, suggesting T_c has little effect on the NCF's microstructure (Fig. 6a). The Raman spectra in Fig. 6b indicates an increase in G band intensity (and a decreased I_D/I_G ratio) correlated with increasing T_c up to 800 °C, suggesting the formation of more graphitic-like domains and, consequently, improved electronic conductivity at higher carbonization temperature (inset in Fig. 6b). The FTIR results in Fig. 6c also show that lower carbonization temperatures (in the range 600–700 °C) do not affect the intensity

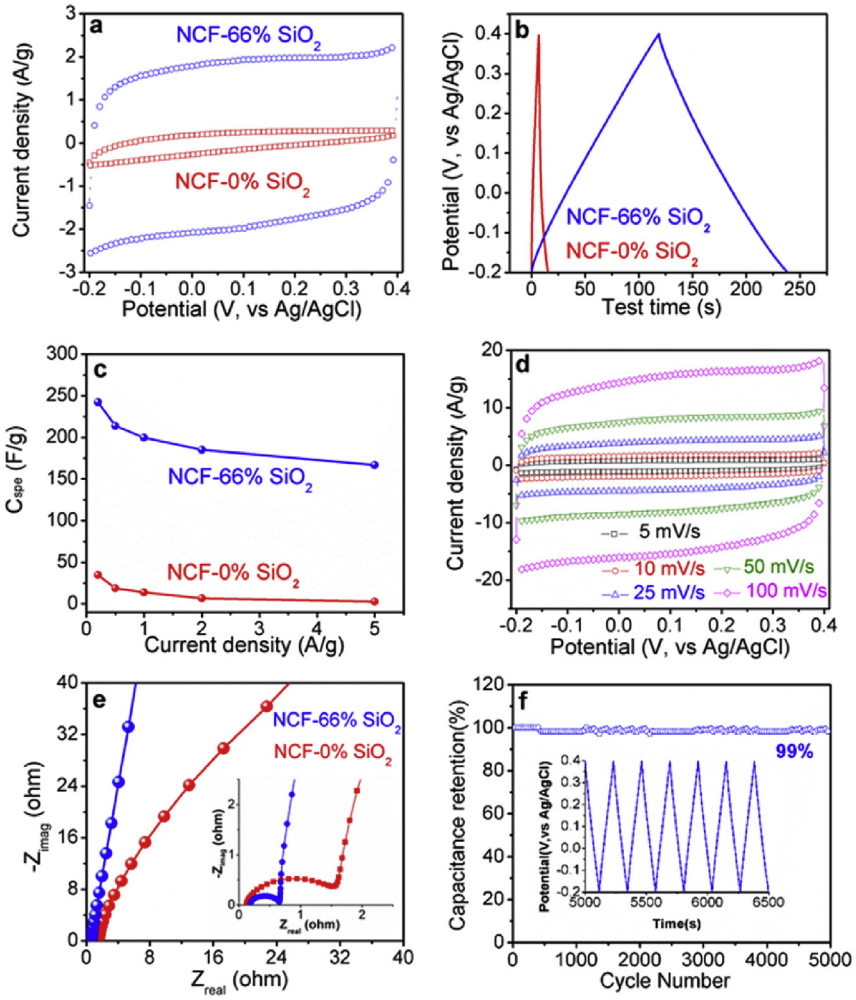

Fig. 3. (a) CV curves for NCF-66% SiO_2 and NCF-0% SiO_2 in 1 M H_2SO_4 solution between −0.2 and 0.4 V. (b) GCD curves of NCF-66% SiO_2 and NCF-0% SiO_2 at the current density of 1 A/g. (c) The specific capacity of NCF-66% SiO_2 and NCF-0% SiO_2 at various current densities. (d) CV curves of NCF-66% SiO_2 at different scan rates. (e) Nyquist plots of NCF-66% SiO_2 and NCF-0% SiO_2 (The inset is the EIS plot in the high frequency region). (f) Cycling performance for NCF-66% SiO_2 at 1 A/g for 5000 cycles (The inset is a portion of the charge-discharge curves). (A colour version of this figure can be viewed online.)

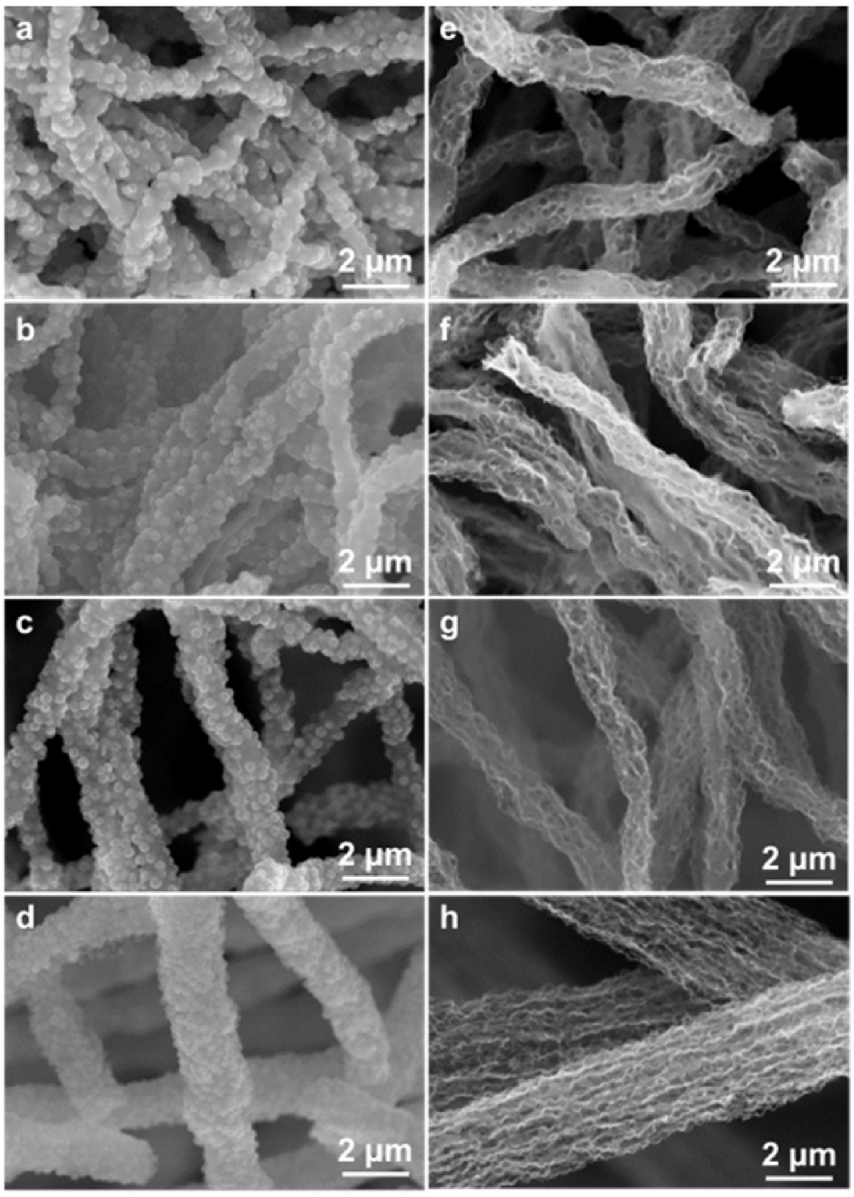

Fig. 4. SEM images of fibers before (a–d) and after SiO_2 spheres removal (e–h) at different SiO_2 mass percentage: (a,e) 33%; (b,f) 50%; (c,g) 66%; (d,h) 75%. (A colour version of this figure can be viewed online.)

or position of the peaks. However, for the NCFs that were carbonized at higher temperatures (>800 °C), the intensity of all peaks (1060–1696 cm^{-1}) was greatly weakened, suggesting that higher T_c substantially removed the most disordered carbon. This led to the graphitic ordering, and most likely originates from the dangling bonds and functionalities. The EDX analysis of NCF in Fig. 6d also suggests that higher T_c is responsible for lower nitrogen content and the ordered graphitic domains in Fig. 6b. For instances, the

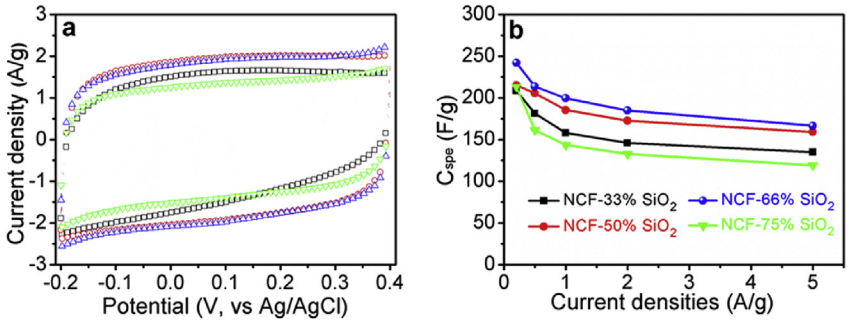

Fig. 5. (a) CV curves for different NCF in 1 M H_2SO_4 solution at a scan rate of 10 mV/s. (b) The specific capacity of different NCFs at various current densities. (A colour version of this figure can be viewed online.)

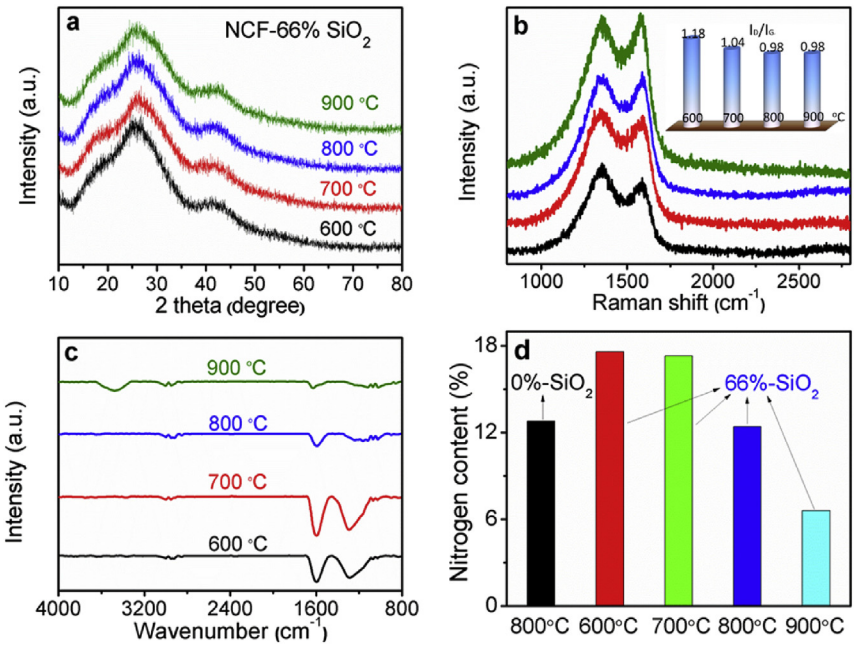

Fig. 6. (a) XRD, (b) Raman, (c) FTIR spectra and (d) nitrogen content of NCF-66% SiO_2 prepared under different carbonization temperatures. The inset in Fig. 6b is I_D/I_G ratio changes with the temperature increase. (A colour version of this figure can be viewed online.)

nitrogen content is almost constant up until $T_c = 700$ °C (17.3 wt%), and drops to 12.4 wt% and 6.6 wt% at $T_c = 800$ °C and 900 °C, respectively. It's worth mentioning that doping the carbon materials with enriched nitrogen species are commonly achieved by carbonizing the nitrogen-containing resins, such as melamine-resorcinol-formaldehyde [36,44], or by post-annealing the carbon materials in ammonium [45]. These processes are either complicated, time-consuming or have strict operation conditions. On the other hand, we were able to produce nitrogen-enriched carbon fibers with functionalities content up to 17.3 wt% by a simple pyrolysis of a PAN-based polymer fiber. According to the literature, pyridinic-N, pyrrolic-N and pyridone-N can provide pseudocapacitance through the redox reactions involving protons [46–48]. Although Béguin et al. obtained nitrogen-enriched CNF (13 wt% of nitrogen) similarly followed by CO_2 activation, our NCF possesses higher nitrogen content and excellent electrochemical performances despite their low SSA (<60 m^2/g) [21]. Moreover, the meso-macroporous hierarchical channels greatly facilitate the ion diffusion kinetics, resulting in a high rate handling properties in the NCF. Said otherwise, quite comparable electrochemical performances could be obtained in the low surface area, nitrogen-enriched carbon fiber networks, while at the same time eliminates the time consuming, complicated post fiber activation procedure, which usually boosts the SSA at the expenses of introducing impurities and discounted electronic conductivity.

The effect of T_c on the electrochemical performances of NCF was studied and shown in Fig. 7a. Increasing the T_c up to 800 °C dramatically enlarges the encircled CV area and results in a smaller time constant (qualitatively judged from the CV shape), which is indicative of higher specific capacitance and improved rate capability. Since the 600 °C and 700 °C samples possessed quite similar nitrogen content and SSA, the remarkable capacitance enhancement in the latter can be attributed to its more developed graphitized domains (Fig. 6b). Nevertheless, likely due to the discontinuous electron transport paths as a result of excessive doped nitrogen species, both the 600 °C and 700 °C samples display fast capacitance decay as the current densities are elevated. On the other hand, carbonizing the polymer mat at 800 °C could retain moderate-high nitrogen content (12.4 wt%) and developed graphitized domains, leading to excellent rate capability (Fig. 7b). Higher

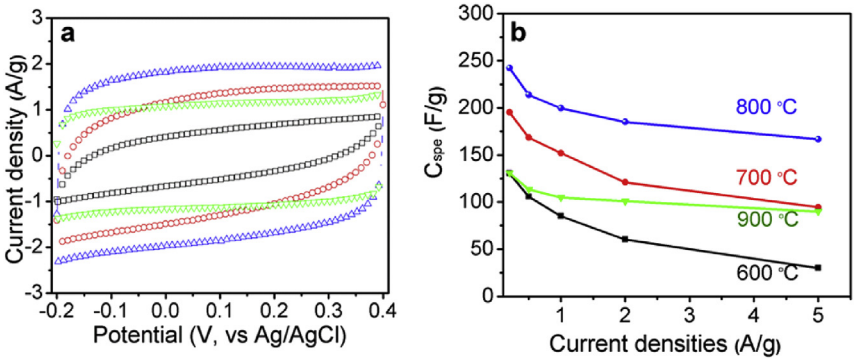

Fig. 7. (a) CV curves for NCF-66% SiO_2 obtained at different temperatures in 1.0 M H_2SO_4 solution at 10 mV/s. (b) The specific capacity for NCF-66% SiO_2 obtained at different temperatures at various current densities. (A colour version of this figure can be viewed online.)

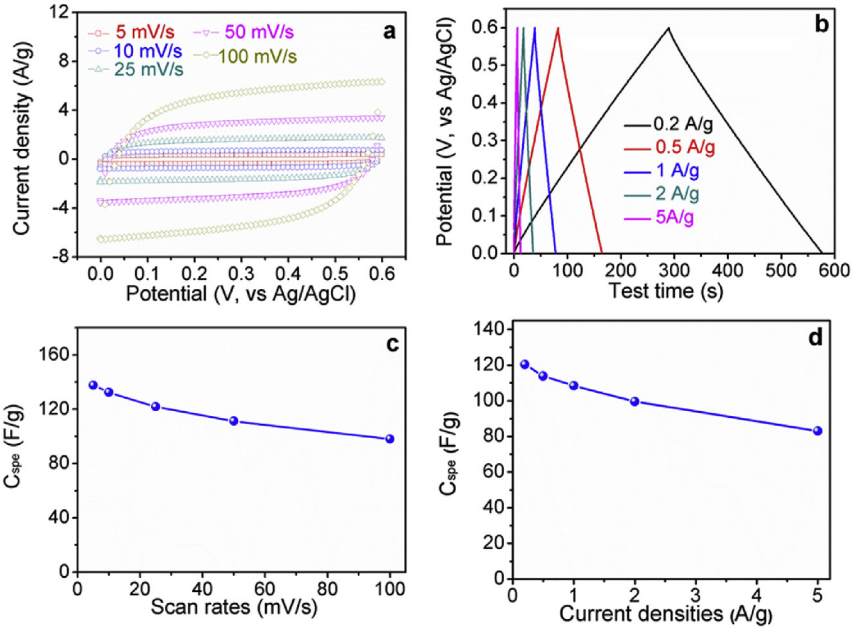

Fig. 8. (a, b) CV curves and GCD curves for NCF-66% SiO_2 tested in a two electrode system. (c, d) The specific capacity of NCF-66% SiO_2 at different scan rates and current densities in a two-electrode system. (A colour version of this figure can be viewed online.)

carbonization temperature (900 °C) greatly reduces the doped nitrogen species to 6.6 wt% (Fig. 6d), thus leading to a much lower pseudocapacitance.

The optimized binder-free electrodes (66% SiO_2, 800 °C) were further assembled into symmetric supercapacitors. The electrochemical performances were evaluated through CV and GCD tests as shown in (Fig. 8a–b). The device exhibits a rectangular CV shape at all scan rates with rapid current responses upon voltage reversal (Fig. 8a) and symmetric, linear GCD profiles at all current densities with a small IR drop (Fig. 8b), thus demonstrating purely capacitive behaviors and high-rate responses. The capacitances normalized to single electrodes are 138 F/g at 5 mV/s and 98 F/g at 100 mV/s, which are comparable to the values derived from the discharge curves (Fig. 8c–d).

4. Conclusions

In summary, we demonstrate a facile strategy to prepare nitrogen-enriched carbon fibers (NCF). The as-prepared flexible, self-sustaining NCF exhibit a thin carbon layer morphology and possess low surface area (<60 m^2/g), meso-macroporous nanostructure, and high nitrogen content (as high as 17.3 wt%). Benefiting from the shortened ion diffusion path and redox-active nitrogen species, the NCF display high pseudocapacitance (242 F/g at 0.2 A/g), fast rate-responses, and stable cycling lifetime (99% of initial capacitance after 5000 cycles) coupled with purely capacitive behaviors. Moreover, the double-layer capacitance and pseudocapacitance could be easily decoupled. The SiO_2 content in the blended precursor solution as well as the carbonization temperature were determined to be of critical importance in the physical properties and electrochemical performances of the resulted NCFs. When assembled into a symmetric device, the NCF-based supercapacitor exhibits 138 F/g at 5 mV/s and 98 F/g at 100 mV/s. These promising results represent the potential of this binder-free, flexible NCF in capacitive energy storage systems, whose performance can be promoted in further steps by additional investigation.

Acknowledgements

The authors gratefully acknowledge financial support from the National Natural Science Foundation of China (NO. 21001091, 21273004 and 21073156), the Project Funded by the Priority Academic. We would also like to acknowledge the technical support received at the testing center of Yangzhou University. Dr Sang Hoon Park from Trinity College Dublin was acknowledged for useful data discussions.

Appendix A. Supplementary data

Supplementary data related to this article can be found at http://dx.doi.org/10.1016/j.carbon.2016.06.067.

References

[1] P. Simon, Y. Gogotsi, Materials for electrochemical capacitors, Nat. Mater 7 (11) (2008) 845–854.
[2] D.N. Futaba, H. Kenji, Y. Takeo, H. Tatsuki, H. Yuhei, K. Yozo, et al., Shape-engineerable and highly densely packed single-walled carbon nanotubes and their application as super-capacitor electrodes, Nat. Mater 5 (12) (2006) 987–994.
[3] J.S. Huang, B.G. Sumpter, M. Vincent, Theoretical model for nanoporous carbon supercapacitors, Angew. Chem. Int. Ed. 47 (3) (2008) 520–524.
[4] D. Bhattacharjya, M.S. Kim, T.S. Bae, J.S. Yu, High performance supercapacitor prepared from hollow mesoporous carbon capsules with hierarchical nano-architecture, J. Power Sources 244 (4) (2013) 799–805.
[5] Q. Wang, J. Yan, T. Wei, J. Feng, Y. Ren, Z. Fan, et al., Two-dimensional mesoporous carbon sheet-like framework material for high-rate supercapacitors, Carbon 60 (12) (2013) 481–487.
[6] C. Vix-Guterl, E. Frackowiak, K. Jurewicz, M. Friebe, J. Parmentier, F. Béguin, Electrochemical energy storage in ordered porous carbon materials, Carbon 43 (6) (2005) 1293–1302.
[7] J. Hu, Z. Kang, F. Li, X. Huang, Graphene with three-dimensional architecture for high performance supercapacitor, Carbon 67 (67) (2014) 221–229.
[8] C. Zhang, K.B. Hatzell, M. Boota, B. Dyatkin, M. Beidaghi, D. Long, et al., Highly porous carbon spheres for electrochemical capacitors and capacitive flowable suspension electrodes, Carbon 77 (10) (2014) 155–164.
[9] O. Barbieri, M. Hahn, A. Herzog, R. Kötz, Capacitance limits of high surface area activated carbons for double layer capacitors, Carbon 43 (6) (2005) 1303–1310.
[10] L. Kong, C. Zhang, S. Zhang, J. Wang, R. Cai, C. Lv, et al., High-power and high-energy asymmetric supercapacitors based on Li^+-intercalation into a *T*-Nb_2O_5/

graphene pseudocapacitive electrode, J. Mater Chem. A 2 (2014) 17962–17970.
[11] C.C. Hu, W.C. Chen, K.H. Chang, How to achieve maximum utilization of hydrous ruthenium oxide for supercapacitors, J. Electrochem Soc. 151 (2004) A281–A290.
[12] T. Brousse, R. Marchand, P.L. Taberna, P. Simon, TiO_2 (B)/activated carbon nonaqueous hybrid system for energy storage, J. Power Sources 158 (1) (2006) 571–577.
[13] D.W. Wang, F. Li, Z.G. Chen, G.Q. Lu, H.M. Cheng, Synthesis and electrochemical property of boron-doped mesoporous carbon in supercapacitor, Chem. Mat. 20 (22) (2008) 7195–7200.
[14] Z. Zhou, Y.R. Zhu, Z.B. Wu, F. Lu, M.J. Jing, X.B. Ji, Amorphous RuO_2 coated on carbon spheres as excellent electrode materials for supercapacitors, RSC Adv. 4 (2014) 6927–6932.
[15] M. Zhou, F. Pu, Z. Wang, S. Guan, Nitrogen-doped porous carbons through koh activation with superior performance in supercapacitors, Carbon 68 (3) (2013) 185–194.
[16] R. Marcus, K. Yair, K. Emanuel, B. Lars, O. Martin, K. Stefan, et al., Hierarchical micro- and mesoporous carbide-derived carbon as a high-performance electrode material in supercapacitors, Small 7 (8) (2011) 1108–1117.
[17] C.F. Zhang, Y.B. Xie, M.Q. Zhao, A.E. Pentecost, Z. Lin, J.T. Wang, et al., Enhanced electrochemical performance of hydrous RuO_2/mesoporous carbon nanocomposites via nitrogen doping, ACS Appl. Mater Interfaces 6 (12) (2014) 9751–9759.
[18] H. Niu, J. Zhang, Z. Xie, X. Wang, T. Lin, Preparation, structure and supercapacitance of bonded carbon nanofiber electrode materials, Carbon 49 (7) (2011) 2380–2388.
[19] S.H. Yoon, S. Lim, S. Yan, Y. Ota, W. Qiao, A. Tanaka, et al., KOH activation of carbon nanofibers, Carbon 42 (8–9) (2004) 1723–1729.
[20] R. Liu, L. Pan, J. Jiang, X. Xi, X. Liu, D. Wu, Nitrogen-doped carbon microfiber with wrinkled surface for high performance supercapacitors, Sci. Rep. 6 (2016) 21750.
[21] E.J. Ra, E. Raymundo-Piñero, Y.H. Lee, F. Béguin, High power supercapacitors using polyacrylonitrile-based carbon nanofiber paper, Carbon 47 (13) (2009) 2984–2992.
[22] Z.R. Ismagilov, A.E. Shalagina, O.Y. Podyacheva, A.V. Ischenko, L.S. Kibis, A.I. Boronin, et al., Structure and electrical conductivity of nitrogen-doped carbon nanofibers, Carbon 47 (8) (2009), 1922–9.
[23] Y. Cheng, L. Huang, X. Xiao, B. Yao, L. Yuan, T. Li, et al., Flexible and cross-linked N-doped carbon nanofiber network for high performance freestanding supercapacitor electrode, Nano Energy 15 (2015) 66–74.
[24] C. Ma, Y. Song, J. Shi, D. Zhang, X. Zhai, M. Zhong, et al., Preparation and one-step activation of microporous carbon nanofibers for use as supercapacitor electrodes, Carbon 51 (1) (2013) 290–300.
[25] C. Kim, Electrochemical characterization of electrospun activated carbon nanofibres as an electrode in supercapacitors, J. Power Sources 142 (1) (2005) 382–388.
[26] D. Li, Y.N. Xia, Electrospinning of nanofibers: reinventing the wheel, Adv. Mater 16 (2004) 1151–1170.
[27] A. Greiner, J.H. Wendorff, Electrospinning: a fascinating method for the preparation of ultrathin fibers, Angew. Chem. Int. Ed. 46 (30) (2007) 5670–5703.
[28] E. Zussman, R. Avrahami, M. Feldman, Electrospun polyaniline/poly(methyl methacrylate)-derived turbostratic carbon micro/nanotubes, Adv. Mater 18 (3) (2006) 348–353.
[29] J.G. Wang, Y. Yang, Z.H. Huang, F. Kang, A high-performance asymmetric supercapacitor based on carbon and carbon–MnO_2 nanofiber electrodes, Carbon 61 (11) (2013) 190–199.
[30] N.C. Abeykoon, J.S. Bonso, J.P. Ferraris, Supercapacitor performance of carbon nanofiber electrodes derived from immiscible PAN/PMMA polymer blends, RSC Adv. 5 (2015) 19865–19873.
[31] G.H. An, H.J. Ahn, Activated porous carbon nanofibers using Sn segregation for high-performance electrochemical capacitors, Carbon 65 (6) (2013) 87–96.
[32] S. Mitani, S.I. Lee, K. Saito, S.H. Yoon, Y. Korai, I. Mochida, Activation of coal tar derived needle coke with K_2CO_3, into an active carbon of low surface area and its performance as unique electrode of electric double-layer capacitor, Carbon 43 (14) (2005) 2960–2967.
[33] C. Zhang, Y. Gogotsi, Y. Xie, G. Sun, A. Pentecost, J. Wang, et al., Ion intercalation into graphitic carbon with a low surface area for high energy density supercapacitors, J. Electrochem Soc. 161 (10) (2014) A1486–A1494.
[34] B.J. Ji, Z. Qiao, I. Lee, M. Dahl, F. Zaera, Y. Yin, Mesoporous anatase titania hollow nanostructures though silica-protected calcination, Adv. Funct. Mater 22 (1) (2012) 166–174.
[35] M. Vijayakumar, B. Schwenzer, S. Kim, Z. Yang, S. Thevuthasan, J. Liu, et al., Investigation of local environments in Nafion–SiO_2 composite membranes used in vanadium redox flow batteries, Solid State Nucl. Magn. Reson 42 (2011) 71–80.
[36] H.C. Chen, F.G. Sun, J.T. Wang, W.C. Li, W.M. Qiao, L.C. Ling, et al., Nitrogen doping effects on the physical and chemical properties of mesoporous carbons, J. Phys. Chem. C 117 (16) (2013) 8318–8328.
[37] J.W. Kim, V. Augustyn, B. Dunn, The effect of crystallinity on the rapid pseudocapacitive response of Nb_2O_5, Adv. Energy Mater 2 (1) (2012) 141–148.
[38] A. Veronica, C. Jérémy, M.A. Lowe, W.K. Jong, T. Pierre-Louis, S.H. Tolbert, et al., High-rate electrochemical energy storage through Li^+ intercalation pseudocapacitance, Nat. Mater 12 (6) (2013) 518–522.
[39] W. Lee, J.H. Moon, Monodispersed N-doped carbon nanospheres for supercapacitor application, ACS Appl. Mater Interfaces 6 (16) (2014) 13968–13976.
[40] G.A. Ferrero, A.B. Fuertes, M. Sevilla, N-doped porous carbon capsules with tunable porosity for high-performance supercapacitors J, Mater. Chem. A 3 (2015) 2914–2923.
[41] B. Qiu, C. Pan, W. Qian, Y. Peng, L. Qiu, F. Yan, Nitrogen-doped mesoporous carbons originated from ionic liquids as electrode materials for supercapacitors, J. Mater Chem. A 1 (21) (2013) 6373–6378.
[42] D. Hulicova-Jurcakova, M. Seredych, Q.L. Gao, T.J. Bandosz, Combined effect of nitrogen- and oxygen-containing functional groups of microporous activated carbon on its electrochemical performance in supercapacitors, Adv. Funct. Mater 19 (3) (2009) 438–447.
[43] X. Yang, D. Wu, X. Chen, R. Fu, Nitrogen-enriched nanocarbons with a 3D continuous mesopore structure from polyacrylonitrile for supercapacitor application, J. Phys. Chem. C 114 (2010) 8581–8586.
[44] H.H. Zhou, S. Xu, H.P. Su, M. Wang, W.M. Qiao, L.C. Ling, et al., Facile preparation and ultra-microporous structure of melamine-resorcinol-formaldehyde polymeric microspheres, ChemCommun 49 (36) (2013) 3763–3765.
[45] W. Luo, B. Wang, C.G. Heron, M.J. Allen, J. Morre, C.S. Maier, et al., Pyrolysis of cellulose under ammonia leads to nitrogen-doped nanoporous carbon generated through methane formation, Nano Lett. 14 (4) (2014) 2225–2229.
[46] G. Lota, K. Lota, E. Frackowiak, Nanotubes based composites rich in nitrogen for supercapacitor application, Electrochem Commun. 9 (7) (2007) 1828–1832.
[47] E. Frackowiak, Carbon materials for supercapacitor application, Phys. Chem. Chem. Phys. 9 (15) (2007) 1774–1785.
[48] E. Frackowiak, G. Lota, J. Machnikowski, C. Vix-Guterl, F. Béguin, Optimisation of supercapacitors using carbons with controlled nanotexture and nitrogen content, Electrochim Acta 51 (11) (2006) 2209–2214.